Parametric amplification of optical phonons

A. Cartella[a,1], T. F. Nova[a,b], M. Fechner[a], R. Merlin[c], and A. Cavalleri[a,b,d]

[a]Condensed Matter Dynamics Department, Max Planck Institute for the Structure and Dynamics of Matter, 22761 Hamburg, Germany; [b]The Hamburg Centre for Ultrafast Imaging, University of Hamburg, 22761 Hamburg, Germany; [c]Department of Physics, University of Michigan, Ann Arbor, MI 48109-1040; and [d]Department of Physics, Clarendon Laboratory, University of Oxford, OX1 3PU Oxford, United Kingdom

Edited by Peter T. Rakich, Yale University, New Haven, CT, and accepted by Editorial Board Member Anthony Leggett October 22, 2018 (received for review June 6, 2018)

We use coherent midinfrared optical pulses to resonantly excite large-amplitude oscillations of the Si–C stretching mode in silicon carbide. When probing the sample with a second pulse, we observe parametric optical gain at all wavelengths throughout the reststrahlen band. This effect reflects the amplification of light by phonon-mediated four-wave mixing and, by extension, of optical-phonon fluctuations. Density functional theory calculations clarify aspects of the microscopic mechanism for this phenomenon. The high-frequency dielectric permittivity and the phonon oscillator strength depend quadratically on the lattice coordinate; they oscillate at twice the frequency of the optical field and provide a parametric drive for the lattice mode. Parametric gain in phononic four-wave mixing is a generic mechanism that can be extended to all polar modes of solids, as a means to control the kinetics of phase transitions, to amplify many-body interactions or to control phonon-polariton waves.

phonon amplification | ultrafast spectroscopy | silicon carbide

Amplification of light through stimulated emission or nonlinear optical interactions has had a transformative impact on modern science and technology. The amplification of other bosonic excitations is likely to open up new remarkable physical phenomena. In particular, the amplification of both acoustic and optical phonons under intense laser and magnetic fields (1–4), as well as through Cerenkov effects (5) has long been the subject of theoretical studies. Acoustic phonon amplification has been reported in optically excited ruby (6, 7) and semiconductor superlattices driven by electrical currents (8–10), and is a standard working regime of cavity optomechanics (11). The amplification of optical phonons was so far observed only due to drifting electrons in semiconductor nanostructures (12), where the conditions for Cerenkov amplification are favored. Furthermore, stimulated Brillouin and Raman scattering (13) experiments could lead to the amplification of acoustic and optical phonons, respectively. However, the literature so far focused on the Brillouin and Raman amplification of light, for example in silicon (14, 15).

Here, we explore the nonlinear response of resonantly driven optical phonons in dielectrics; we discuss their amplification and their coupling to electromagnetic radiation.

Fig. 1 depicts the nonlinear dependence of the polarization P on the phonon displacement Q and on an external electric field E in a chain of Si and C atoms. The response of this idealized chain was computed by first-principle calculations. The polar optical mode of this chain involves the relative displacement of the silicon (red) and carbon (blue) sublattices (Fig. 1*A*), reminiscent of the in-plane mode of hexagonal SiC (see below).

The first contribution to the nonlinear polarization, which we will refer to as P_L, bears on the effective dipolar charge Z^*. Such Born effective charge, defined as $Z^* = \partial P_L/\partial Q$, is approximated by a constant in the linear response regime ($P_L = Z^* Q$) but depends on Q for large lattice distortions (Fig. 1 *B* and *C*). For the chain of Fig. 1*A* and, generally, for most dielectrics, the Born effective charge depends quadratically on the lattice coordinate $Z^* = Z_0^* + \alpha Q^2$ (Fig. 1*C*).

The second contribution to the nonlinear polarization emerges from the dielectric screening of the electric field E by the electrons, giving the term $P_\infty = \epsilon_0 \chi E = \epsilon_0(\varepsilon_\infty - 1)E$. In contrast to the Born effective charge, which is a pure ionic response, the permittivity ε_∞ accounts for higher-energy excitations of the electronic band structure such as interband transitions. Similar to the Born effective charge, the permittivity ε_∞ is a constant for small lattice displacements but becomes dependent on Q when the lattice is strongly distorted and hence the band structure changes. This effect is captured by the calculations of Fig. 1*D* for the Si–C chain, in which the slope $\chi = \varepsilon_\infty - 1$ of the polarization $P_\infty = \epsilon_0 \chi E$ is shown to change at large values of Q. This second nonlinear term scales also quadratically with Q, as $\varepsilon_\infty = 1 + \chi = 1 + \partial P_\infty/\partial E = \varepsilon_{\infty,0} + \beta Q^2$ (Fig. 1*E*).

Summarizing, the nonlinear polarization of a strongly driven optical mode in SiC (and a generic dielectric) includes two nonlinear corrections, both quadratic in Q, one to the effective dipolar charge Z^* and one to the dielectric constant ε_∞. Let us now consider the dynamical response of the lattice to an optical field $E = E_0 \sin(\omega t)$, tuned at or near the resonance associated with the transverse optical mode (Fig. 2).

For small field amplitudes, $P = Z_0^* Q + \epsilon_0(\varepsilon_{\infty,0} - 1)E$ and the time-dependent phonon coordinate $Q(t)$ follows the familiar equation of motion of a periodically driven damped oscillator $\ddot{Q} + \Gamma\dot{Q} + \Omega_{TO}^2 Q = Z^* E_0 \sin(\omega t)$, in which Γ and Ω_{TO} denote damping and phonon frequency, respectively. In this case one obtains the familiar linear response expression $Q = Q_0 \sin(\omega t)\exp(-\Gamma t)$.

We first analyze the nonlinear response of P_L alone, that is, when the Born effective charge (but not ε_∞) depends on the lattice displacement ($\alpha \neq 0, \beta = 0$). The equation of motion is $\ddot{Q} + \Gamma\dot{Q} + \Omega_{TO}^2 Q = (Z_0^* + 3\alpha Q^2)E_0 \sin(\omega t)$. To leading order, the

Significance

The amplification of light through stimulated emission or nonlinear optical interactions has had a transformative impact on modern science and technology. The amplification of other bosonic excitations, like phonons in solids, is likely to open up new remarkable physical phenomena. This paper reports an experimental demonstration of optical phonon amplification, supported by first-principle calculations. The combination of our experiments and simulations clarifies a microscopic mechanism for phonon-mediated four-wave mixing, a highly interesting process. Our results could be extended toward an enhanced control of phonon-polariton waves, interesting for information transport on subwavelength length scales.

Author contributions: A. Cartella, R.M., and A. Cavalleri designed research; A. Cartella, T.F.N., and M.F. performed research; A. Cartella analyzed data; and A. Cartella and A. Cavalleri wrote the paper.

The authors declare no conflict of interest.

This article is a PNAS Direct Submission. P.T.R. is a guest editor invited by the Editorial Board.

[1]To whom correspondence should be addressed. Email: andrea.cartella@mpsd.mpg.de.

This article contains supporting information online at www.pnas.org/lookup/suppl/doi:10.1073/pnas.1809725115/-/DCSupplemental.

Published online November 14, 2018.

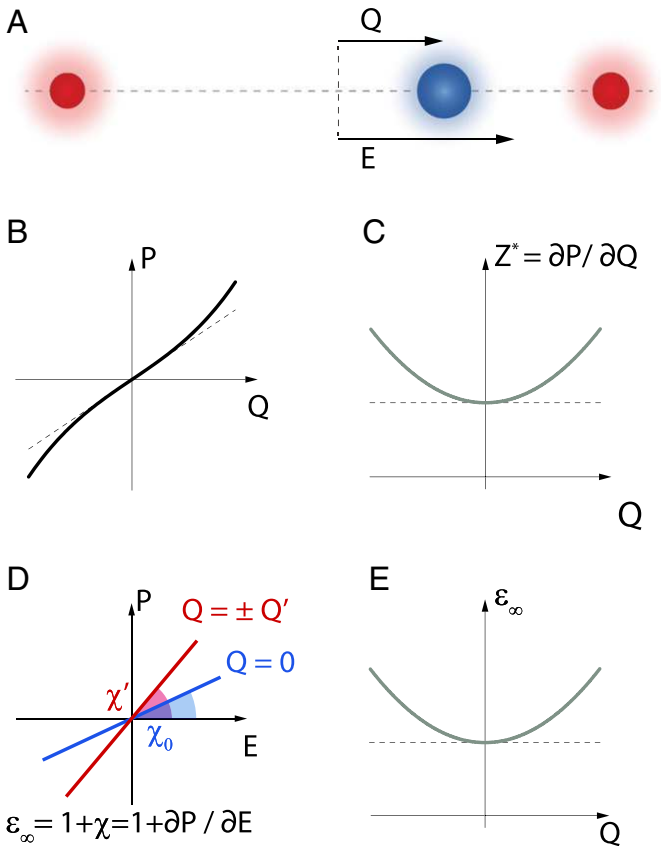

Fig. 1. (*A*) Chain of silicon (blue) and carbon (red) atoms. At equilibrium, the positive ions are surrounded by negative electronic clouds, arranged in space so that no polarization is present. If an ion is displaced, a polarization P is created along the chain. The system can be described by effective positive and negative ionic charges Z^*, depicted as shaded areas around the ions. (*B*) Lattice polarization along the chain and (*C*) effective charge Z^* as a function of Q, resulting from first-principle DFT calculations. For large displacements, the polarization is not linear in Q anymore, and the effective charge is increased. The first expansion of Z^* in Q is parabolic (gray line). (*D*) Nonresonant contribution to the polarization as a function of E for different values of Q. (*E*) Dielectric constant ε_∞ as a function of Q, also parabolic, resulting from first-principle DFT calculations.

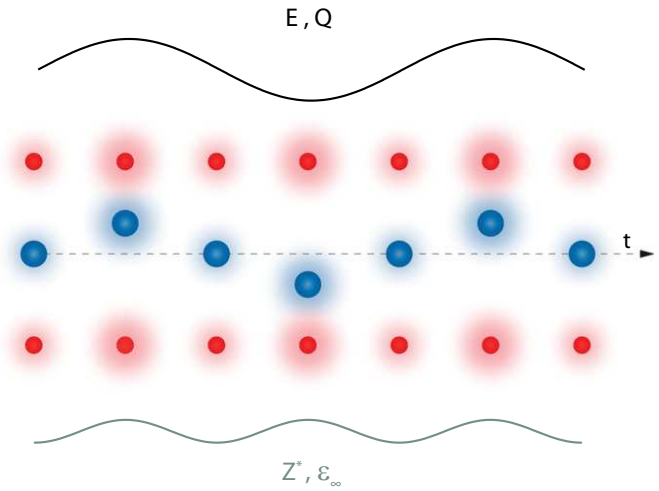

Fig. 2. Dynamical response of the diatomic chain to a large-amplitude periodic driving of the phonon. For an applied electric field $E = E_0 \sin \omega t$ (black line), the phonon coordinate Q oscillates as $Q = Q_0 \sin \omega t$. Due to their quadratic dependence on Q, the effective charge Z^* and the dielectric constant ε_∞(gray line) are oscillating at frequency 2ω.

solution to this equation can be thought of as generating a set of harmonics in the force term. For oscillations in Q at frequency ω, the Born effective charge oscillates at 2ω, as $Z^* = Z_0^* + \alpha Q^2 \sim Z_0^* + \alpha Q_0^2(1/2 - 1/2\cos(2\omega t))$ (Fig. 2). As a consequence, the driving force in the equation of motion includes also a 3ω component as $3\alpha Q^2 E_0 \sin(\omega t) \sim 3\alpha Q_0^2(1/2 - 1/2\cos(2\omega t))E_0 \sin(\omega t)$.

More important is the nonlinear response of $P_\infty = \epsilon_0(\varepsilon_{\infty,0} + \beta Q^2 - 1)E$ to the driving field (α=0,$\beta \neq 0$). This term translates into a $+\epsilon_0 \beta Q^2 E$ correction to the polarization and, thus, into a change in the energy of the system $\Delta U = -PE \propto -\beta Q^2 E^2$. Hence, an additional force emerges on the oscillator $F_Q = -\partial U/\partial Q \propto +\beta E^2 Q$. The equation of motion can therefore be written as $\ddot{Q} + \Gamma \dot{Q} + \Omega(t)_{TO}^2 Q = Z^* E_0 \sin(\omega t)$, with a time-dependent phonon eigenfrequency $\Omega_{TO} = \Omega_{TO,0} - \beta E(t)^2$. Because Ω_{TO} oscillates at frequency 2ω, the equation of motion is that of a forced parametric oscillator. Parametric amplification of lattice fluctuations $Q(t)$ are then expected due to the nonlinearity of P_∞. For a detailed derivation of the nonlinear equations of motion we refer the reader to *SI Appendix*, section S5.

In this work, we experimentally validate the prediction of phonon amplification in bulk silicon carbide (polytype 4H, Fig. 3*A*). If the specific sample crystal structure and dielectric properties are taken into account, the considerations made for the idealized chain of Si and C atoms reported above are still valid (see *SI Appendix*, section S4 for more details). The eigenvector of the phonon studied here is shown in Fig. 3*B*, which displays motions of the Si and C atoms in opposite directions along one of the in-plane crystallographic axes. The equilibrium linear reflectivity is reproduced in Fig. 3*C*, displaying a 5-THz-wide reststrahlen band, between Ω_{TO} = 24 THz and Ω_{LO} = 29 THz. Large-amplitude oscillations of the lattice were driven with midinfrared pulses, which were generated with two optical parametric amplifiers (OPAs) and difference frequency generation (DFG), powered by a Ti:Sa femtosecond laser at 1-KHz repetition rate. The pump pulses were tuned to Ω_{LO} = 29 THz. At these frequencies, the pump pulses were focused to obtain ~9-MV/cm field strengths. A second independently tunable OPAs and DFG setup was used to probe the spectral response of

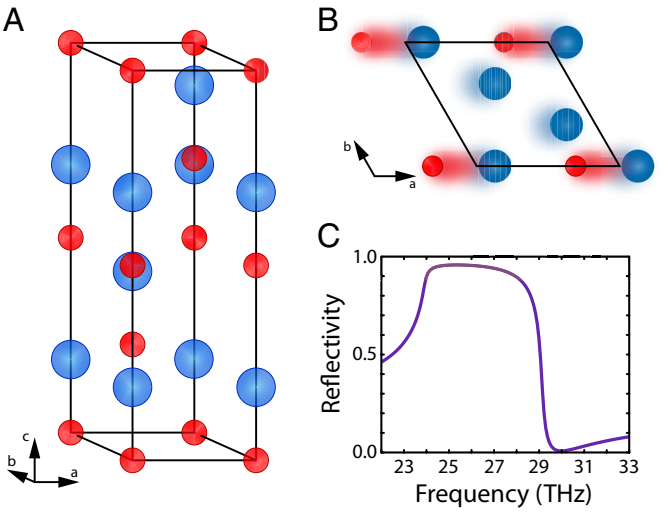

Fig. 3. (*A*) Crystal structure of SiC, polytype 4H (space group C^4_{6v}-$P6_3mc$). Si atoms in blue, C atoms in red. (*B*) Eigenvectors of the infrared active mode excited by the pump pulse (E_u symmetry). (*C*) Reflectivity at equilibrium associated to the driven mode [data from literature (24)].

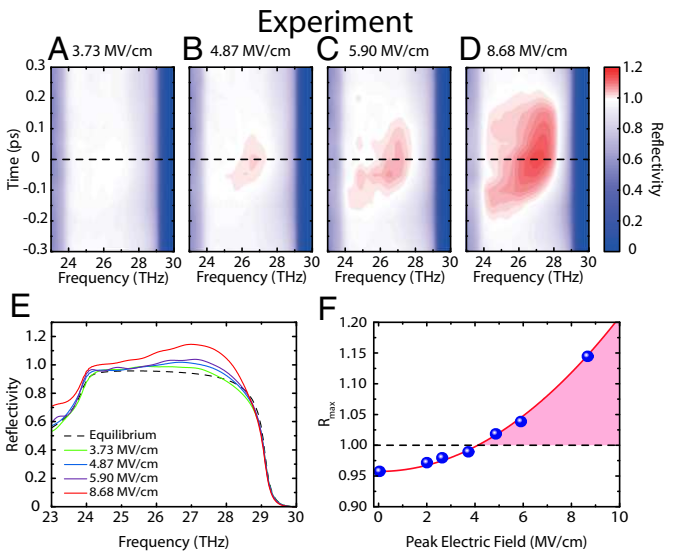

Fig. 4. (*A–D*) Time-delay-dependent and frequency-dependent measured reflectivity $R(t, \omega)$ for driving peak electric fields of (*A*) 3.73, (*B*) 4.87, (*C*) 5.90, and (*D*) 8.68 MV/cm. The color scale is chosen to emphasize in red the regions where the reflectivity is greater than one. The horizontal dashed lines indicate the time delay at which the line-cuts are displayed in *E*. This is the delay at which the highest reflectivity was measured for the highest peak electric field (*D*). (*E*) Frequency-dependent measured reflectivity at the maximum of the pump–probe response for different driving peak electric fields, compared with the equilibrium one (dashed line). (*F*) Peak field dependence of the maximum measured reflectivity. In this plot, two additional data points are shown, corresponding to 2.01 and 2.64 MV/cm. The red line depicts a parabolic fit to the data. More information on the data analysis can be found in the *SI Appendix*, section S2.

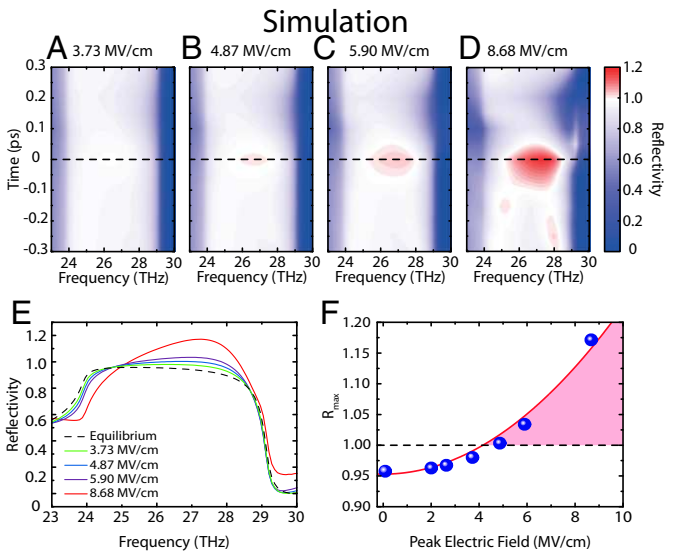

Fig. 5. (*A–D*) Time-delay-dependent and frequency-dependent simulated reflectivity $R(t, \omega)$ for driving peak electric fields of (*A*) 3.73, (*B*) 4.87, (*C*) 5.90, and (*D*) 8.68 MV/cm. The color scale is chosen to emphasize in red the regions where the reflectivity is greater than one. The horizontal dashed lines indicate the time delay at which the line-cuts are displayed in *E*. (*E*) Frequency-dependent calculated reflectivity at the maximum of the pump–probe response for different driving peak electric fields, compared with the equilibrium one (dashed line). (*F*) Peak field dependence of the maximum calculated reflectivity. In this plot, two additional data points are shown, corresponding to 2.01 and 2.64 MV/cm. The red line depicts a parabolic fit to the data.

the same pumped resonance in reflection geometry. The time-resolved reflectivity was recorded with broadband probe pulses centered at 26.5 THz, with spectral weight covering the whole reststrahlen band. As the probe pulses exhibited a stabilized carrier-envelope phase, the time-dependent optical properties could be measured with sensitivity to both amplitude and phase by electrooptic sampling. To sample at this frequency, we compressed the pulses from the titanium:sapphire laser using a near-infrared noncollinear OPA, which generated pulses with ∼20-fs pulse duration (see *SI Appendix*, section S1 for details). The results of our pump–probe experiments are reported in Fig. 4, in which we plot the wavelength-dependent reflectivity after excitation with pump pulses.

For pump electric fields $E_0 > 4$ MV/cm, the reflectivity in the reststrahlen band was observed to become larger than $R = 1$, reaching the values of $R \sim 1.15$ and evidencing amplification. This feature, emphasized in red in Fig. 4 *A–D*, developed at the earliest time delays and at the center of the reststrahlen band, broadening in frequency and persisting for longer time delays as the pump field was increased toward 9 MV/cm. As depicted in Fig. 4*E*, the reflectivity increases throughout the reststrahlen band, scaling quadratically with the pump electric field, as shown in Fig. 4*F*. These observations suggest that for large coherent excitations of the phonon, the probe electric field is amplified and, by extension, the lattice coordinate Q.

Numerical simulations of the optical response under the conditions of the experiment were used to analyze the results above and to validate amplification of both E and Q. Starting from Maxwell's equations, we considered the interaction of electromagnetic transients of arbitrary shape and amplitude with the SiC crystal. In these calculations, which are discussed in *SI Appendix*, section S5, we considered both pump (strong) and probe (weak) pulses and included the quadratic dependence of both the Born effective charge Z^* and dielectric constant ε_∞ on the phonon coordinate Q, as obtained from density functional theory (DFT) analysis of the Si–C lattice.

The calculated α- and β-coefficients were adjusted to fit the experimental data. These simulations reproduced well the main features of the time-delay-dependent and frequency-dependent reflectivity response measured experimentally, as reported in Fig. 5 *A–D*. For pump fields in excess of 4 MV/cm, the simulations predict $R > 1$. Precisely as observed in the experiments, the frequency-dependent profile of the amplification ($R > 1$) emerges from the center of the reststrahlen band and expands both in frequency and time as the pump field increases (Fig. 5*E*). The calculated maximum reflectivity also scales quadratically with the pump peak electric field (Fig. 5*F*), in agreement with the experiments. The simulations further confirm that not only the probe electric field (Fig. 6*A*), but also the oscillations in the phonon coordinate Q (Fig. 6*B*) are amplified. In particular, Fig.

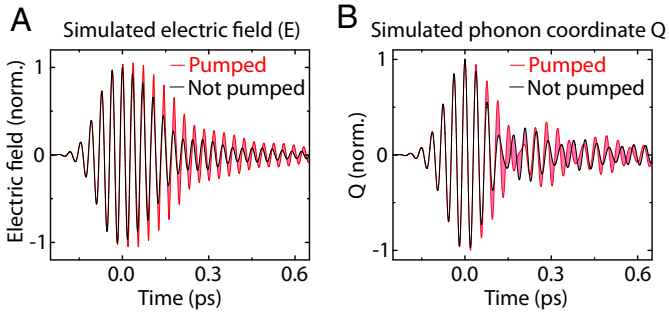

Fig. 6. Probe pulse electric field and phonon amplification. Simulated (*A*) electric field E and (*B*) oscillations of the phonon coordinate Q at the sample surface, driven by a weak probe pulse, with (red solid lines) and without (black solid lines) pump. The shaded areas highlight the amplification.

6*B* displays the time-dependent $Q(t)$ with (red) and without (black) excitation, highlighting phonon amplification.

The idea that lattice fluctuations can be amplified parametrically through the nonlinear response of the lattice is relevant in more than one area. For example, in the context of light-enhanced superconductivity in cuprates (16–18) and in the doped fullerites (19), a recent theory has suggested that parametric amplification of pairs of squeezed phonons may enhance the superconducting instability (20, 21). Integral to these conjectures is the ability to parametrically amplify phonons by four-wave vibrational mixing. The mechanism discussed here naturally extends to these conditions.

The present results are also connected to previous studies in charge-density wave systems, in which parametric amplification of the order-parameter phase mode, driven by large-amplitude coherent excitations of the amplitude mode, has been discussed (22).

Finally, the physics of phonon amplification discussed here could be immediately extended to the manipulation of phonon-polariton waves, which are of interest to information transport on subwavelength length scales (23). The ability to control the properties and amplitude of phonon-polaritons may for example lead to tunable metalenses for the phonon field, or to many other extensions of optoelectronic manipulation to "polaritonics."

ACKNOWLEDGMENTS. The research leading to these results has received funding from the European Research Council (ERC) under the European Union's Seventh Framework Programme (FP7/2007-2013)/ERC Grant Agreement 319286 (Q-MAC).

1. Miranda LCM (1976) Phonon damping in the simultaneous presence of intense radiation and magnetic fields. *J Phys C Solid State Phys* 9:2971–2976.
2. Nunes OAC (1984) Amplification of acoustic lattice vibrations by electrons in semiconductors under intense laser radiation. *J Appl Phys* 56:2694–2696.
3. Nunes OAC (1984) Carrier-assisted laser pumping of optical phonons in semiconductors under strong magnetic fields. *Phys Rev B Condens Matter* 29:5679–5682.
4. Tronconi AL, Nunes OAC (1986) Theory of the excitation and amplification of longitudinal-optical phonons in degenerate semiconductors under an intense laser field. *Phys Rev B Condens Matter* 33:4125–4128.
5. Komirenko SM, Kim KW, Kochelap VA, Koroteev VV, Stroscio MA (2003) Nonlinear regimes of coherent optical phonon generation in quantum wells under electric current pumping. *Phys Rev B Condens Matter Mater Phys* 68:155308.
6. Tilstra L, Arts A, de Wijn H (2003) Coherence of phonon avalanches in ruby. *Phys Rev B Condens Matter Mater Phys* 68:144302.
7. Tilstra LG, Arts AFM, De Wijn HW (2007) Optically excited ruby as a saser: Experiment and theory. *Phys Rev B Condens Matter Mater Phys* 76:024302.
8. Shinokita K, et al. (2016) Strong amplification of coherent acoustic phonons by intraminiband currents in a semiconductor superlattice. *Phys Rev Lett* 116:075504.
9. Beardsley RP, Akimov AV, Henini M, Kent AJ (2010) Coherent terahertz sound amplification and spectral line narrowing in a stark ladder superlattice. *Phys Rev Lett* 104:085501.
10. Beardsley RP, Campion RP, Glavin BA, Kent AJ (2011) A GaAs/AlAs superlattice as an electrically pumped THz acoustic phonon amplifier. *New J Phys* 13:073007.
11. Aspelmeyer M, Kippenberg TJ, Marquardt F (2014) Cavity optomechanics. *Rev Mod Phys* 86:1391–1452.
12. Liang W, et al. (2003) Observation of optical phonon instability induced by drifting electrons in semiconductor nanostructures. *Appl Phys Lett* 82:1968–1970.
13. Boyd RW (2008) *Nonlinear Optics* (Academic, New York), 3rd Ed.
14. Kittlaus EA, Shin H, Rakich PT (2016) Large Brillouin amplification in silicon. *Nat Photonics* 10:463–467.
15. Claps R, Dimitropoulos D, Raghunathan V, Han Y, Jalali B (2003) Observation of stimulated Raman amplification in silicon waveguides. *Opt Express* 11:1731–1739.
16. Hu W, et al. (2014) Optically enhanced coherent transport in YBa2Cu3O6.5 by ultrafast redistribution of interlayer coupling. *Nat Mater* 13:705–711.
17. Kaiser S, et al. (2014) Optically induced coherent transport far above Tc in underdoped YBa2Cu2O6+x. *Phys Rev B Condens Matter Mater Phys* 89:184516.
18. Mankowsky R, et al. (2017) Optically induced lattice deformations, electronic structure changes, and enhanced superconductivity in $YBa_2Cu_3O_{6.48}$. *Struct Dyn* 4:044007.
19. Mitrano M, et al. (2016) Possible light-induced superconductivity in K3C60 at high temperature. *Nature* 530:461–464.
20. Knap M, Babadi M, Refael G, Martin I, Demler E (2016) Dynamical Cooper pairing in nonequilibrium electron-phonon systems. *Phys Rev B* 94:214504.
21. Murakami Y, Tsuji N, Eckstein M, Werner P (2017) Nonequilibrium steady states and transient dynamics of conventional superconductors under phonon driving. *Phys Rev B* 96:045125.
22. Liu HY, et al. (2013) Possible observation of parametrically amplified coherent phasons in K0.3MoO3 using time-resolved extreme-ultraviolet angle-resolved photoemission spectroscopy. *Phys Rev B Condens Matter Mater Phys* 88:045104.
23. Dai S, et al. (2014) Tunable phonon polaritons in atomically thin van der Waals crystals of boron nitride. *Science* 343:1125–1129.
24. Spitzer WG, Kleinman D, Walsh D (1959) Infrared properties of hexagonal silicon carbide. *Phys Rev* 113:127–132.